

Conformational Conversion May Precede or Follow Aggregate Elongation on Alternative Pathways of Amyloid Protofibril Formation

Santosh Kumar and Jayant B. Udgaonkar*

National Centre for Biological Sciences, Tata Institute of Fundamental Research, Bangalore 560 065, India

Received 17 July 2008;
received in revised form
14 November 2008;
accepted 15 November 2008
Available online
25 November 2008

A major goal in the study of protein aggregation is to understand how the conformational heterogeneity characteristic of the process leads to structurally distinct amyloid fibrils. The small protein barstar is known to form amyloid protofibrils in multiple steps at low pH: a small oligomer, the A-form, first transforms into a larger spherical higher oligomeric intermediate (HOI), which then self-associates to form the elongated protofibril. To determine how the conformational conversion reaction during aggregation is coupled to the process of protofibril formation, cysteine-scanning mutagenesis was first used to identify specific residue positions in the protein sequence, which are important in defining the nature of the aggregation process. Two classes of mutant proteins, which are distinguished by their kinetics of aggregation at high protein concentration, have been identified: Class I mutant proteins undergo conformational conversion, as measured by an increase in thioflavin T binding ability and an increase in circular dichroism at 216 nm, significantly faster than Class II mutant proteins. At low protein concentration, the rates of conformational conversion are, however, identical for both classes of mutant proteins. At high protein concentration, the two classes of mutant proteins can be further distinguished on the basis of their rates of protofibril growth, as determined from dynamic light-scattering measurements. For Class I mutant proteins, protofibril elongation occurs at the same, or slightly faster, rate than conformational conversion. For Class II mutant proteins, protofibril elongation is significantly slower than conformational conversion. Dynamic light scattering measurements and atomic force microscopy imaging indicate that for the Class I mutant proteins, conformational conversion occurs concurrently with the self-association of prefibrillar HOIs into protofibrils. On the other hand, for the Class II mutant proteins, the prefibrillar HOI first undergoes conformational conversion, and the conformationally converted HOIs then self-associate to form protofibrils. The two classes of mutant proteins appear, therefore, to use structurally distinct pathways to form amyloid protofibrils. On one pathway, conformational conversion occurs along with, or after, elongation of the oligomers; on the other pathway, conformational conversion precedes elongation of the oligomers. Single mutations in the protein can cause aggregation to switch from one pathway to the other. Importantly, the protofibrils formed by the two classes of mutant proteins have significantly different diameters and different internal structures.

© 2008 Elsevier Ltd. All rights reserved.

Edited by J. Weissman

Keywords: barstar; amyloid protofibrils; soluble oligomers; conformational conversion; alternative pathways

*Corresponding author. E-mail address: jayant@ncbs.res.in.

Abbreviations used: HOI, higher oligomeric intermediate; AFM, atomic force microscopy; ThT, thioflavin T; wt, wild type; DLS, dynamic light scattering.

Introduction

Virtually any protein can self-assemble into amyloid fibrils,¹ and structural heterogeneity is the hallmark of virtually all protein aggregation reactions leading to the formation of amyloid fibrils. Heterogeneity is evident in the different sizes of oligomers that are populated transiently during fibril formation and in the variety of structures (spherical, annular, and worm-like) that these oligomers adopt.^{2–12} Heterogeneity is evident in the structures of amyloid fibrils themselves.^{2,13–17} While the cross- β motif is a feature common to all amyloid fibrils,^{18,19} its exact molecular structure can show variations. A protein can form amyloid fibrils of multiple distinct conformations, not only in response to a change in either fibril growth conditions^{13,20,21} or the amino acid sequence of the protein¹⁴ but also under a single growth condition.^{2,15} Understanding the origin of the conformational polymorphism seen in amyloid fibril structures, in terms of the underlying mechanism of self-assembly, is a major goal of protein aggregation studies.

The roles of prefibrillar spherical oligomers in the assembly of elongated worm-like protofibrils (whose ends can sometimes close to form annular rings²²), as well as of long, straight fibrils, are still poorly understood. An important question is whether the conformational conversion reaction leading to the characteristic increase in β -sheet structure occurs in prefibrillar spherical oligomers or in elongated protofibrillar structures, both of which have been implicated as toxic entities in diseases related to amyloid fibril formation.^{1,23–25} Determining whether fibrillation drives conformational conversion, or whether conformational conversion drives fibrillation, will help in delineating the pathways of fibrillation^{5,7,21,26–28} and the possible roles of alternative pathways in giving rise to alternative conformational variants of amyloid protofibrils and fibrils.^{2,14,21,29} Understanding how alternative pathways of aggregation originate, how they differ in intermediate aggregate structures and in the sequence of steps involved, and how aggregation may switch from one available pathway to another is necessary, for example, for understanding strain diversity and amyloidosis in the case of prion protein.^{30–32}

Like many other proteins, the small protein barstar forms soluble oligomers (the A form), as well as amyloid protofibrils and fibrils, at low pH. The A form of barstar is a symmetrical aggregate formed by the self-assembly of about 16 protein molecules.^{33,34} NMR characterization of the A form has shown that the core of the aggregate is formed by the C-terminal segments of the 16 self-assembled protein molecules.³⁵ The A form transforms into amyloid protofibrils in a slow stepwise process that is accelerated at higher temperatures.^{12,36} The amyloid protofibrils of barstar are elongated worm-like fibrils, and atomic force microscopy (AFM) studies suggest that they are assemblies of the A form oligomers.^{11,12} Time-resolved fluorescence studies have suggested that

the cores of the aggregates in the A form oligomers and in the protofibrils are similar.¹¹ This report presents the results of a cysteine-scanning mutagenesis study that investigates the effects of mutations on the kinetics of protofibril formation from the A form. The advantage of using cysteine, instead of proline or alanine, in scanning mutagenesis is that the thiol group of a cysteine can be easily modified. If a site-specific effect on aggregation kinetics is observed upon replacement of an amino acid residue by cysteine, it then becomes easy to obtain further structural information on the importance of the residue position by suitable chemical modification of the cysteine thiol.

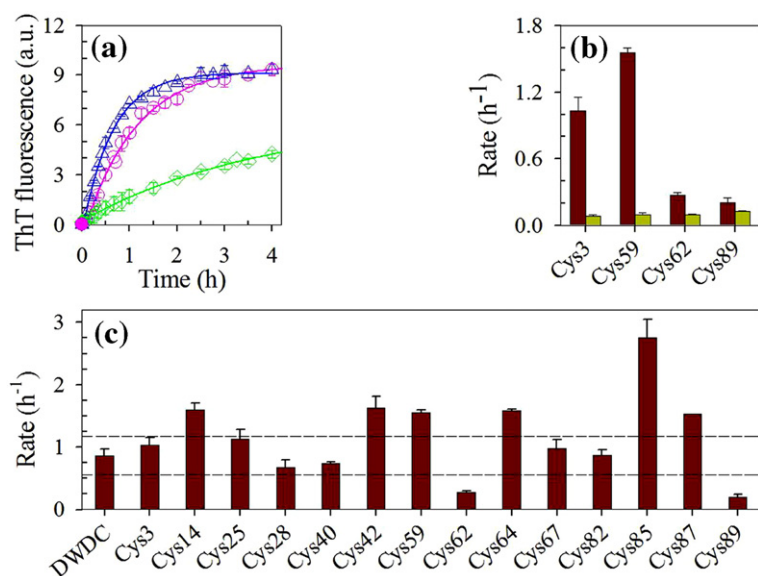
The cysteine-scanning mutagenesis study shows that the kinetics of formation of protofibrils from the A form are highly dependent on the position of the mutation. It is seen that single point mutations can lead to the formation of amyloid protofibrils of distinct conformations. The use of multiple structural probes to monitor the kinetics of protofibril formation by a few representative mutant proteins suggests that the formation of distinct protofibril conformations occurs *via* alternative pathways. The sequence of events occurring and differentiating the alternative pathways is described. It appears that single mutations can cause the process of aggregation to switch between alternative pathways and can thereby change the conformation of the amyloid protofibrils formed.

Results

Effect of mutations on the kinetics of amyloid protofibril formation

Figure 1a shows representative data for three different mutant variants of barstar showing that the kinetics of protofibril formation determined by the thioflavin T (ThT) binding assay are monophasic, with no lag phase, as seen previously for wild-type (wt) barstar.¹² Although similar amplitudes of fluorescence change are observed, the observed rate depends on the position of mutation when the concentration of the aggregating protein is 20 μ M, but not when it is lower at 5 μ M (Supporting Information, Fig. S1; Fig. 1b). The high reproducibility of the data is indicated by the small error in measurement at each time point. Importantly, overlapping kinetic curves are obtained when samples are spun at 20,000g for 2 min prior to the ThT assay, and when they are not, indicating that there are no large insoluble aggregates interfering with any of the spectroscopic measurements (data not shown).

The kinetics of protofibril formation by 15 single cysteine-containing mutant variants of barstar, when determined at the higher protein concentration (20 μ M), are found to be monophasic, with no lag phase (Fig. S2). The aggregation kinetics fit reasonably well to a single-exponential equation, even though the aggregation reaction is complex and not



different mutant variants of barstar at 20 μM . Dashed lines span the ± 3 SD spread around the mean rate observed for DWDC, determined from three independent experiments. Error bars represent either the standard deviations obtained from three separate experiments or the spread in the values obtained from two independent experiments.

first-order. The observed rates are similar (Cys3, Cys25, Cys28, Cys40, Cys67, and Cys82), faster (Cys14, Cys42, Cys59, Cys64, Cys85, and Cys87), or slower (Cys62 and Cys89) than that observed for DWDC (the pseudo-wt parent sequence; see [Materials and Methods](#)) (Fig. 1c). The mutations affect the β -sheet propensity, hydrophobicity, and stability of the protein, but no correlations between these physicochemical properties and the kinetics of aggregation were found (Fig. S3). A possible reason for the absence of an expected correlation^{38–40} is that the different mutant proteins form protofibrils through different pathways.

Mutant proteins can be categorized into two classes

Four different structural probes were used to study the kinetics of protofibril formation by DWDC and four representative mutant forms of barstar at the higher protein concentration (20 μM) (Fig. S4). In

addition to ThT fluorescence, changes in ellipticity at 216 nm (CD_{216}), which, similar to ThT fluorescence, probe the internal conformational change during aggregation; the mean hydrodynamic radius (R_H), which reports on the growth (elongation) of aggregates; and the total scattering intensity (SI), which indicates both the size and the amount of aggregates, were measured. For each of the mutant proteins and for each of the probes, the kinetics were found to be monophasic, with no lag phase, and exponential fits to the kinetic data points were extrapolated (at $t=0$) to the value of the signal expected for the A form (Figs. S2 and S4), suggesting, as it did in case of the wt protein,^{11,12} that the A form acts as the direct precursor for protofibril formation. Apparent rates obtained from single exponential fits are shown in Fig. 2.

Figure 2 suggests two classes of mutant proteins. For Class I mutant proteins (DWDC, Cys3, and Cys59) (Fig. 2a–c), the R_H -monitored kinetics are similar to or faster (1.5-fold) than the kinetics

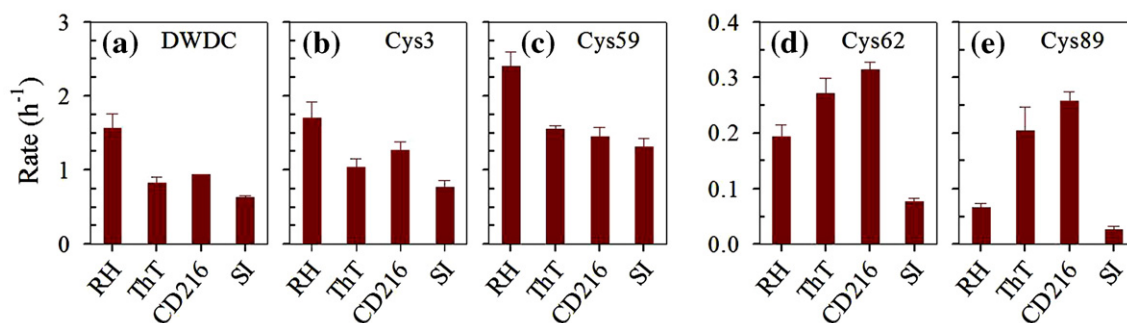


Fig. 2. Probe dependences of the observed rates of amyloid protofibril formation by DWDC (a) and four representative mutant variants of barstar (b–e). Aggregation was carried out at a protein concentration of 20 μM at pH 2.7 and 60 $^{\circ}\text{C}$. Error bars represent either the standard deviations obtained from three separate experiments or the spread in the values obtained from two independent experiments.

monitored by ThT fluorescence and CD₂₁₆. In contrast, for Class II mutant proteins (Cys62 and Cys89) (Fig. 2d and e), the ThT fluorescence- and CD₂₁₆-monitored kinetics are faster than the R_H -monitored kinetics. Within Class II, the ThT fluorescence- and CD₂₁₆-monitored kinetics are 1.5-fold and 3.5-fold faster than the R_H -monitored kinetics for Cys62 and Cys89, respectively. The SI-monitored kinetics are similar to the kinetics monitored by ThT fluorescence and CD₂₁₆ for the Class I mutant proteins, but are drastically (>5-fold) slower for the Class II mutant proteins (Fig. 2).

Aggregates formed by the two classes of mutant proteins are structurally distinct

For further studies, DWDC and Cys3 were chosen as representative Class I mutant proteins, and Cys62 and Cys89 were chosen as representative Class II mutant proteins. The aggregates formed by the two classes of mutant proteins were characterized at a time corresponding to three time constants of the ThT fluorescence-monitored kinetics ($3\tau_{cc}$), when the internal conformational change (conformational conversion) occurring during the process, as monitored by both ThT fluorescence- and CD₂₁₆-monitored kinetics, is complete (Fig. 2). The observation that the final ThT fluorescence signal is the same for aggregates of both classes (Fig. 3a) indicates that similar amounts of aggregate are formed by all

proteins. Hence, the observation that the CD₂₁₆ signal of Class II aggregates is significantly lower than that of the Class I aggregates (Fig. 3b) at $3\tau_{cc}$ must mean that the aggregates formed in similar amounts have dissimilar structures. In this context, the observation that the CD₂₁₆ signal, as well as the shape, of the CD spectra of the aggregates of both classes does not change upon further heating for a time corresponding to $6\tau_{cc}$ (Fig. 3b, inset) is important. For all mutant proteins, the CD spectra of the aggregates show a minimum at 212 nm, at $3\tau_{cc}$ and $6\tau_{cc}$. It should also be noted that, for all the aggregates, troughs in the CD spectra are quite broad, indicating that the protein in the aggregates is not pure β -sheet. For the aggregation of the Class II proteins, the SI increases by about 2-fold from $3\tau_{cc}$ to $6\tau_{cc}$ (Fig. S4); hence, the observation that the CD spectra remain the same indicates that the spectra are not affected by light scattering. Consequently, it is unlikely that the difference seen in the CD spectra of the Class I and Class II aggregates at $3\tau_{cc}$ is an artifact due to light scattering.

Figure 3c shows that the R_H distributions at $3\tau_{cc}$ are monomodal for both classes of mutant proteins. Importantly, the distributions corresponding to Class II aggregates show greater heterogeneity and partially overlap with the A form distribution (Fig. 3c, inset), which is indicative of the presence of smaller aggregates. When the percent scattering intensity distributions are converted into percent mass distri-

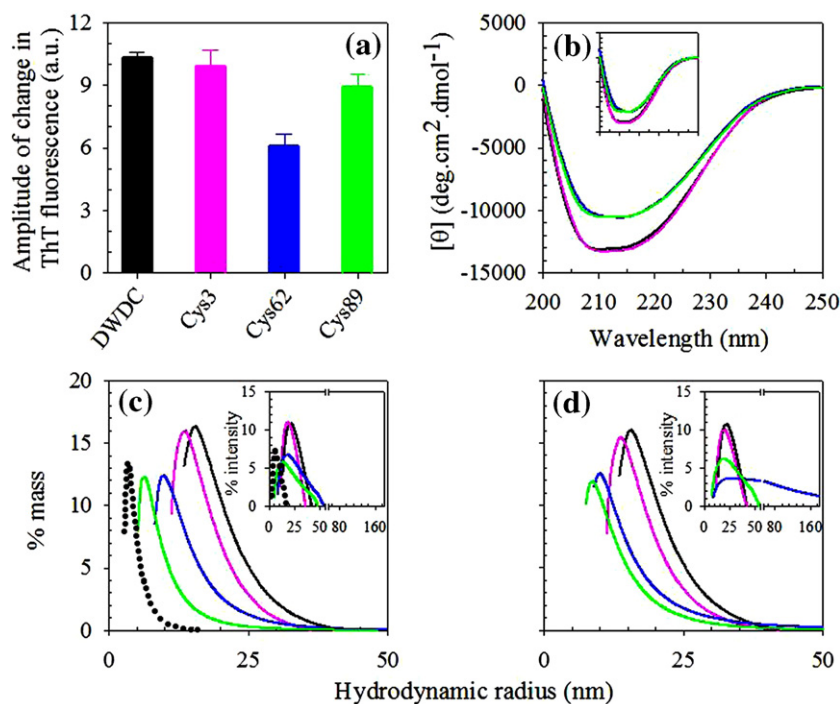


Fig. 3. Spectroscopic characterization of the aggregates formed after completion of conformational conversion. Aggregation was carried out at a protein concentration of 20 μ M at pH 2.7 and 60 $^{\circ}$ C. Measurements were performed at a time corresponding to three time constants ($3\tau_{cc}$) (a–c) and six time constants ($6\tau_{cc}$) (d) of the ThT fluorescence-monitored kinetics. (a) Amplitude of the change in ThT fluorescence. (b) Far-UV CD spectra at $3\tau_{cc}$. The inset shows the far-UV CD spectra at $6\tau_{cc}$. For the calculation of the mean residual ellipticity $[\theta]$, the protein concentration taken was the monomer concentration. (c) Distributions of hydrodynamic radii (at $3\tau_{cc}$) in terms of percent mass. The peak positions are 15 nm, 13.5 nm, 9.8 nm, and 6.4 nm, respectively, for DWDC, Cys3, Cys62, and Cys89. The inset shows the corresponding distributions in terms of percent scattering intensity. The

peak positions, obtained from percent scattering intensity distributions, are 21.1 nm, 18.1 nm, 18.1 nm, and 12.8 nm, respectively, for DWDC, Cys3, Cys62, and Cys89. (d) Distributions of hydrodynamic radii (at $6\tau_{cc}$) in terms of percent mass. The peak positions are 15 nm, 13.5 nm, 9.8 nm, and 9 nm, respectively, for DWDC, Cys3, Cys62, and Cys89. The inset shows corresponding distributions in terms of percent scattering intensity. The peak positions, obtained from percent scattering intensity distributions, are 21.1 nm, 19.6 nm, 27.1 nm, and 20 nm, respectively, for DWDC, Cys3, Cys62, and Cys89. In (b), (c), and (d), the black, pink, blue, and green lines represent the data for DWDC, Cys3, Cys62, and Cys89, respectively. In (c), the dotted line represents the distribution of the A form formed by Cys89.

butions (Fig. 3c) to correct for the dominance of larger aggregates, Class II aggregates are seen to have smaller hydrodynamic radii than do Class I aggregates. Upon further heating up to time $6\tau_{cc}$ (Fig. 3d),

the distributions are found to be identical with those at $3\tau_{cc}$ for the Class I aggregates. For the Class II aggregates, the peaks of the distributions have shifted towards higher R_H values, suggesting that some

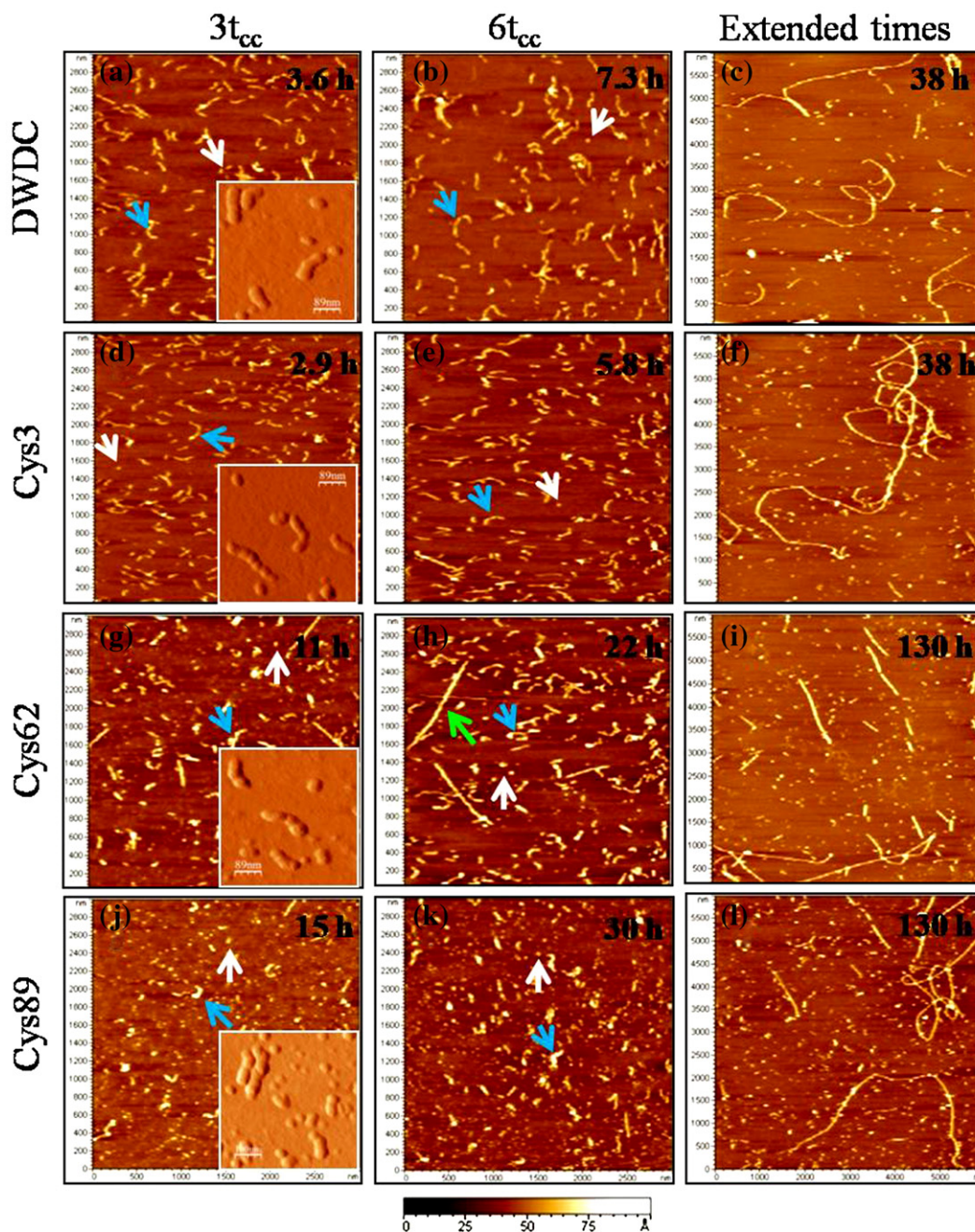


Fig. 4. AFM images of protein aggregates. Protein (20 μM) was heated at 60 $^{\circ}\text{C}$ and pH 2.7. The panels in the leftmost row (a, d, g, j) represent the aggregates formed at a time corresponding to three time constants of the corresponding ThT fluorescence-monitored kinetics ($3\tau_{cc}$; i.e., upon completion of conformational conversion). In (a), (d), (g), and (j), the elongated protofibrils represent approximately 76%, 76%, 33%, and 11% (by number), respectively, of the total number of aggregates observed. The panels in the middle row (b, e, h, k) show the aggregates formed at $6\tau_{cc}$. The white, blue, and green arrows show HOIs, elongated protofibrils, and longer fibrillar structures, respectively. The insets to (a), (d), (g), and (j) show amplitude images of aggregates at higher resolution. The AFM images of the aggregates formed upon prolonged heating (38 h for DWDC and Cys3; 130 h for Cys62 and Cys89) are shown in the rightmost panels (c, f, i, l). The diameters, obtained from height, are $2.0(\pm 0.4)$ nm and $1.8(\pm 0.3)$ nm for the protofibrils formed by DWDC and Cys3, respectively, and are $2.9(\pm 0.5)$ nm and $3.0(\pm 0.6)$ nm for the protofibrils formed by Cys62 and Cys89, respectively. The diameters of the worm-like fibrils (rightmost) formed by DWDC, Cys3, Cys62, and Cys89, as determined from height, are $2.3(\pm 0.5)$ nm, $2.5(\pm 0.3)$ nm, $3(\pm 0.4)$ nm, and $3(\pm 0.4)$ nm, respectively. Note that the scanned area shown in the leftmost and middle panels is $3\ \mu\text{m} \times 3\ \mu\text{m}$, while it is $6\ \mu\text{m} \times 6\ \mu\text{m}$ for the rightmost panels.

growth (elongation) of smaller aggregates into amyloid protofibrils has occurred, but the peaks are still at considerably lower R_H values than those of the Class I aggregates. In the case of Cys62, the distribution at $6\tau_{cc}$ is seen to tail towards higher R_H values, indicating the presence of very large aggregates (Fig. 3d, inset). However, the fraction of these very larger aggregates is very small, as evident in the percent mass distribution (Fig. 3d). It should be mentioned that although Cys59 aggregates faster than do DWDC and Cys3 (Fig. 1), the CD spectra and size distributions of its aggregates were similar to those of these other Class I proteins (data not shown).

Figure 4 shows AFM images of aggregates obtained at different times of the aggregation reaction. At short times, spherical oligomers are seen for both Class I and Class II proteins, which, in agreement with dynamic light-scattering (DLS) experiments, show that the A form is replaced by substantially larger oligomers very early during aggregation (Fig. S5). These spherical oligomers, which assemble progressively into amyloid protofibrils,¹² are referred to as higher oligomeric intermediates (HOIs). At $3\tau_{cc}$, the Class I aggregates (Fig. 4a and d) comprise predominantly of elongated protofibrils and very few HOIs, and the aggregates look similar at $6\tau_{cc}$ (Fig. 4b and e). In contrast, Class II aggregates at $3\tau_{cc}$ (Fig. 4g and j) predominantly comprise HOIs, with relatively few elongated protofibrils. Within this class, Cys62 shows relatively more elongated protofibrils than does Cys89 at $3\tau_{cc}$, and the amounts of elongated protofibrils increase at $6\tau_{cc}$, for both proteins (Fig. 4h and k); these observations are consistent with the R_H distributions (Fig. 3c and d). Cys62 also shows a few long fibrillar structures at $6\tau_{cc}$ (Fig. 4h, green arrow), an observation consistent with the tailing observed at high R_H values in the distribution of hydrodynamic radii (Fig. 3d, inset) (see above). At very long times of aggregation, both Class I and Class II mutant proteins form long worm-like fibrils (Fig. 4c, f, i, and l).

The AFM images also indicate that Class II protofibrils have a diameter that is about 1.5-fold larger than that of Class I protofibrils (Fig. 5; legend to Fig. 4). Hence, Class II protofibrils differ from Class I protofibrils not only in their secondary structural content (Fig. 3b) but also in their size.

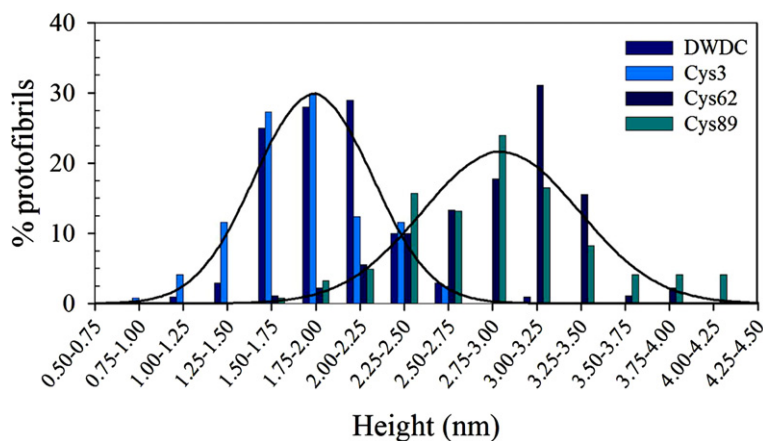


Fig. 5. Distributions of the diameters of protofibrils formed by the Class I (DWDC and Cys3) and Class II (Cys62 and Cys89) mutant proteins. The solid lines are fits to a Gaussian equation.

Discussion

Formation of amyloid protofibrils by barstar occurs *via* higher-order oligomeric intermediates

An earlier study¹² has shown that the A form of wt barstar, a soluble oligomer comprising 16 monomeric units, transforms into amyloid protofibrils in multiple steps. Early during the aggregation process, the A form assembles into spherical HOIs, which then assemble further into protofibrils in a progressive manner, as shown previously for the wt protein¹² and now for all mutant variants, from the DLS-measured R_H distributions (data not shown). At early times ($0.1\tau_{cc}$) of aggregation, spherical HOIs are the predominant aggregates visible in the AFM images, along with very few protofibrils (Fig. S5). The protofibrils seen at $3\tau_{cc}$ have a beaded appearance, suggesting that they have assembled directly from the HOIs (Fig. 4a, d, g, and j, insets). Hence, the assembly of barstar protofibrils occurs *via* the following stages of aggregate growth: native protein \rightarrow A form \rightarrow HOI \rightarrow protofibril. Such a mechanism of assembly *via* oligomeric intermediates, where the growth of aggregates occurs by the association of oligomeric intermediates, appears to be a common mechanism for amyloid protofibril and fibril assembly.^{5,6,8-10}

Stepwise formation of amyloid protofibrils

The formation of amyloid protofibrils involves not only aggregate growth and elongation but also conformational change. An increase in β -sheet structure was seen for the wt protein¹² and is seen for the mutant proteins studied here (Fig. 3). The protein does not, however, convert completely into a β -sheet structure during the conformational conversion reaction: the broad minima in the CD spectra (Fig. 3b) of the aggregate at $3\tau_{cc}$ and $6\tau_{cc}$ indicate that other secondary structures are still present. In the case of wt barstar, it appeared that conformational conversion, the internal conformational change measured by the increase in ThT-binding ability and in the

increase in CD-monitored β -sheet structure, occurs during and after the elongation of the aggregates.¹² Here, a cysteine-scanning mutagenesis approach has been followed to identify residue positions that are important in determining the kinetics of aggregation. Two classes of mutant proteins, which differ in their aggregation rates, have been identified. At high protein concentrations, the majority of mutant proteins (Class I) aggregate at rates similar to or slightly faster than those of the pseudo-wt parent protein, while two mutant proteins (Class II) aggregate at significantly slower rates (Fig. 1c). The observation that the differences in rates disappear when aggregation is carried out at low protein concentrations (Fig. 1b) validates the results of an earlier study¹² indicating that the rate-determining step at low protein concentrations is the association of protein molecules, while the overall rate is limited by an internal conformational change at higher protein concentrations. More importantly, the observation suggests that the Class II mutations perturb the rate of conformational conversion significantly, and hence might uncouple conformational conversion and elongation steps during protofibril formation.

Mechanism of protofibril formation by Class I mutant proteins

The formation of protofibrils by the Class I mutant proteins is complete at the time ($3\tau_{cc}$) the conformational conversion reaction is complete. The R_H distribution does not change from times $3\tau_{cc}$ to $6\tau_{cc}$ (Fig. 3c and d), and the AFM images indicate that no further elongation occurs from times $3\tau_{cc}$ to $6\tau_{cc}$ (Fig. 4). These results suggest that conformational conversion accompanied protofibril elongation and may have even followed protofibril elongation. The latter possibility is, in fact, suggested by the observation that the R_H -monitored kinetics are 1.5-fold faster than the kinetics monitored by ThT fluorescence and CD₂₁₆ (Fig. 2a–c), but because the R_H measurement is biased towards the largest aggregate present at the time of measurement and is not directly proportional to the total amount of aggregated material, the data cannot preclude the possibility that conformational conversion occurs, instead, concurrently with elongation. Hence, protofibril formation by the Class I mutant proteins is similar to that by wt barstar,¹² in which conformational conversion occurs during or after elongation.

For other proteins, too,^{5,8,41} similar observations that the kinetics of elongation are similar to those of conformational conversion have led to the conclusion that conformational conversion occurs concurrently with, and indeed may be driven by, fibrillation. However, in the case of other proteins and barstar, it is possible that conformational conversion occurs within the prefibrillar spherical oligomers (HOIs), which then equilibrate very rapidly with fibrillar aggregates. It would then mistakenly appear that conformational conversion occurs simultaneously with assembly into fibrillar structures when, in reality, it precedes it. The possibility appears, however,

unlikely in the case of barstar because although the AFM images indicate that the diameter of the HOIs increases by about 2-fold from time $0.1\tau_{cc}$ (when they are first seen) to time $3\tau_{cc}$, the DLS-measured R_H distributions indicate that the mean R_H , and hence length, increases progressively during this time (data not shown). Consequently, it appears that conformational conversion either accompanies or follows protofibril assembly.

Mechanism of protofibril formation by Class II mutant proteins

For the Class II mutant proteins, the HOIs are the predominant aggregates at the time ($3\tau_{cc}$) the conformational conversion is complete. Few elongated protofibrils are seen to have formed at time $3\tau_{cc}$ (Fig. 4g and j), and although their number has increased at time $6\tau_{cc}$, as seen in the AFM images (Fig. 4h and k) and in the shift in R_H distributions (Fig. 3c and d), they remain relatively sparsely populated. These results suggest that conformational conversion had already occurred in the HOIs before they assembled into protofibrils. Importantly, the extent of conformational conversion at time $3\tau_{cc}$, as determined from the amplitudes of change in ThT fluorescence (Fig. 3a), is the same as that seen at $3\tau_{cc}$ for the Class I proteins. Not surprisingly then, the R_H - and SI-monitored kinetics are significantly slower than those monitored by ThT fluorescence and CD₂₁₆ (Fig. 2d and e). At the time $3\tau_{cc}$, Cys89 shows relatively fewer elongated protofibrils than Cys62 (Fig. 4g and j), an observation consistent with the differences in growth rates (R_H -monitored kinetics) and conformational conversion rates (ThT fluorescence- and CD₂₁₆-monitored kinetics) observed between the two mutant proteins (Fig. 2d and e).

The sparse accumulation of protofibrils at all times during the aggregation process suggests not only that the transformation of HOIs into protofibrils is slow, as indicated by the slowness of the R_H - and SI-monitored kinetics, but also that the final equilibrium established between the two species favors the HOIs. In contrast, the equilibrium established between the HOIs and protofibrils of the Class I mutant proteins strongly favors the protofibrils.

For both Class I and Class II, the SI-monitored kinetics are slower than the kinetics monitored by mean R_H (Fig. 2). As in the case of wt barstar,¹² this might be suggestive of a lateral association of the elongated protofibrils to form mature amyloid protofibrils. Such lateral association would lead to an increase in scattering intensity without an apparent increase in mean hydrodynamic radius.⁴²

Alternative pathways for protofibril formation

There are two distinct ways by which fibrillar aggregates can elongate. In aggregation processes showing the characteristics of classical nucleated polymerization,^{3,26} elongation seems to occur by the sequential addition of monomeric intermediates

onto the template formed initially in the reaction. When elongation occurs *via* the assembly of oligomeric intermediates,^{7–12} the associating unit is the oligomeric intermediate. In both cases, it has been suggested that the associating units first add onto the ends of growing aggregates and then undergo β -sheet conformational change.^{5,8,41,43}

In the case of barstar, this study, as well as a previous study,¹² has suggested that the associating unit is the spherical HOI, which itself is assembled from the A form oligomer. The observation that the patterns of site-specific side-chain dynamics in the A form and in the protofibrils¹¹ are similar suggests that structures (e.g., monomers) formed by the dissociation of the A form are unlikely to be involved in the formation of protofibrils. It has, however, been difficult to distinguish between two assembly scenarios at the microscopic level: one scenario in which protofibril growth occurs by assembly of HOIs, and another scenario in which the A form oligomers (in equilibrium with the HOI) add onto a protofibril growth site.

This report suggests that there are two fundamentally different routes to assembly *via* oligomeric intermediates (Fig. 6). The Class I mutant proteins are like many other proteins^{5,8,41,43} for which conformational conversion accompanies or

follows assembly of HOIs into protofibrils (Fig. 6a, Pathway I). On the other hand, in the case of the Class II mutant proteins, conformational conversion occurs in the HOIs themselves, and the conformationally converted HOIs assemble into protofibrils (Fig. 6b, Pathway II). Very recently, it has been shown in the case of the amyloid β protein that the assembly of fibrils, too, may involve conformationally converted soluble oligomers,⁴⁴ as has been shown for protofibrils in this study.

It is expected that alternative pathways, which differ in the structures of the oligomeric intermediates that assemble into protofibrils, will lead to protofibrils that differ in structure. At the gross level, this appears to be true for protofibril formation by barstar: the protofibrils formed on Pathway II not only have larger diameters (Fig. 5) but also have significantly different far-UV CD spectra (Fig. 3b). This result needs, however, to be confirmed by higher-resolution structural characterization, and, currently, a hydrogen exchange methodology coupled with mass spectrometry is being used to determine whether the structures are different at even finer detail.

The kinetic measurements used to delineate the two pathways are ensemble measurements, and it is possible, especially given the heterogeneity that is clearly evident in the aggregation reaction, that a fraction of Class I oligomers might use Pathway II to form protofibrils, and that a fraction of Class II oligomers might use Pathway I. But the two pathways lead to fibrils of different sizes, and very few of the protofibrils formed by Class I oligomers have the diameter of protofibrils formed by Class II oligomers, and vice versa (Fig. 5). Hence, it appears that Pathway I is the predominant pathway for Class I oligomers, and that Pathway II is the predominant pathway for Class II oligomers.

In this study, the demonstration of alternative pathways for aggregation involving structurally distinct oligomeric intermediates has important implications. Their existence would explain the structural heterogeneity inherent in the process of amyloid protofibril formation and might represent the origin of prion strain diversity.⁴⁵ Their existence, together with the observation that single point mutations can change the preference of a protein for the available pathways, is of significance for the formulation of therapies against amyloid-related diseases.⁴⁶ Finally, precise control on switching between available pathways that generate different amyloid conformations will be necessary for the formulation of amyloid-based nanomaterials.⁴⁷

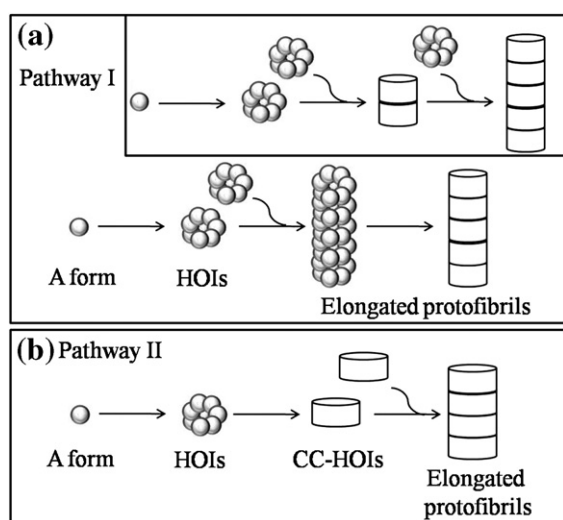


Fig. 6. Multi-pathway mechanism for amyloid protofibril formation. (a) Pathway I: The A form is first converted into HOIs, which then grow in size to form elongated protofibrils. The conformational conversion leading to the formation of ThT binding sites and an increase in β -sheet content seems to occur in these elongated protofibrils. The inset brings out the possibility that conformational conversion may also occur along with growth (elongation). (b) Pathway II [assembly *via* conformationally converted oligomers (ACCO)]: The A form is first converted into HOIs, which undergo conformational conversion to form conformationally converted HOIs (CC-HOIs), which then assemble to form the elongated protofibrils. On both pathways, the elongated protofibrils then seem to associate laterally to form mature amyloid protofibrils. The amyloid protofibrils formed on these alternative pathways differ in their structures.

Materials and Methods

Protein expression and purification

Wild-type barstar has three tryptophan (at positions 38, 44, and 53) and two cysteine (at positions 40 and 82) residues. The DWDC mutant form of barstar has only one tryptophan residue at position 53 and has no cysteine

residue. The single cysteine-containing mutant variants of barstar used in the present study are derived from DWDC and have only one cysteine residue introduced at the position indicated in their names. All the proteins were expressed and purified using the procedure described earlier.³³ The purity of each protein was confirmed to be more than 98% by SDS-PAGE and mass spectrometry using a Micromass Q-TOF Ultima spectrometer. The mutant proteins investigated in this study are as follows: A3C (Cys3), S14C (Cys14), A25C (Cys25), E28C (Cys28), A40C (Cys40), T42C (Cys42), S59C (Cys59), L62C (Cys62), E64C (Cys64), A67C (Cys67), A82C (Cys82), T85C (Cys85), I87C (Cys87), and S89C (Cys89).

Buffers, solutions, and experimental conditions

All reagents used in the study were of the highest purity grade available from Sigma. The protein was first dissolved in 20 mM Tris buffer (pH 8) and then diluted 10-fold into 50 mM glycine buffer (pH 2.7). All the buffers contained 1 mM DTT, except those for the CD measurements, which contained 200 μ M DTT. The protein concentration was determined by measuring absorbance at 280 nm using $\epsilon_{280} = 10,000 \text{ M}^{-1} \text{ cm}^{-1}$.

The aggregation process was monitored at 60 °C by ThT fluorescence, ellipticity at 216 nm (CD_{216}), and DLS measurements. Samples were first incubated for 2 h at pH 2.7 and 25 °C, and then transferred to a heating block set at 60 °C. In all cases, the sample reached the temperature of 60 °C within 3 min of transfer to the heating block. At different times of incubation at 60 °C, aliquots of the samples were withdrawn for spectroscopic measurements.

ThT fluorescence assay

A predetermined amount of aggregating protein was withdrawn, cooled to 25 °C, and then added to the ThT-containing assay solution, so that the final concentrations of protein and dye in the assay solutions were 1 μ M and 5 μ M, respectively. In the assay solution, the pH was adjusted to 8 by mixing the sample aliquot with 50 mM Tris buffer. Fluorescence measurements were carried out on a Fluoromax-3 spectrofluorimeter (Jobin Yvon). The sample was excited at 440 nm, and emission at 482 nm was monitored. The excitation and emission bandwidths were set at 1 nm and 10 nm, respectively.

Determining change in the physicochemical properties of protein upon mutation

The change in hydrophobicity (ΔHydr) upon mutation was calculated using $\Delta\text{Hydr} = (\text{Hydr}_{\text{DWDC}}) - (\text{Hydr}_{\text{Mut}})$. $\text{Hydr}_{\text{DWDC}}$ and Hydr_{Mut} are the hydrophobicities of the parent and mutant residues, respectively. The hydrophobicity value (free energy of transfer from water to *n*-octanol) for each amino acid was taken from White and Wimley.⁴⁸ The change in β -sheet propensity resulting from mutation was calculated using $\Delta\beta\text{-sheet propensity} = P_{\text{DWDC}}^{\beta} - P_{\text{Mut}}^{\beta}$. P_{DWDC}^{β} and P_{Mut}^{β} are the β -sheet propensities of the parent and mutant residues, respectively. The β -sheet propensity value for each amino acid was taken from Street and Mayo.⁴⁹ C_m represents the midpoint of a urea-induced equilibrium unfolding transition and is a measure of the stability of the protein. The C_m values for Cys3, Cys14, Cys25, Cys40, Cys42, Cys67, Cys82, and Cys89 were taken from Jha and Udgaonkar.⁵⁰

Circular dichroism

Far-UV CD measurements were carried out on a Jasco J-720 spectropolarimeter. The spectra were collected using a step resolution of 1 nm, a scan speed of 100 nm/min, and a bandwidth of 1 nm. Each spectrum was averaged over 20 scans. Ellipticity at 216 nm was monitored at different time points for kinetic measurements.

DLS measurements

The DLS experiments were carried out on a DynaPro-99 unit (Protein Solutions Ltd.). All the buffers and pH 8 protein solutions were filtered through a 0.02- μ m filter (Whatman Anodisc 13). A laser of 829.4 nm wavelength was used to illuminate the sample. The scattering intensity at 90° and its autocorrelation function were measured simultaneously. For each time point 20 acquisitions were collected, which were then resolved into Gaussian distributions of hydrodynamic radii by using the regularization algorithm (Protein Solutions Ltd.). Results of the regularization algorithm were also verified by the DynaLS software (Protein Solutions Ltd.). The viscosities of the solutions, used to calculate R_{H} , were determined from the measurements of refractive indices. Total light scattering intensity was determined using cumulants analysis (Protein Solutions Ltd.). Distributions of scattering intensity were converted into distributions of mass using the equation:

$$\% \text{mass} = \left(\frac{A_1}{R_1^3} / \sum \frac{A_i}{R_i^3} \right)$$

where A_i and R_i represent the areas and hydrodynamic radii in the distributions of scattering intensity, respectively.

Atomic force microscopy

AFM imaging was performed using a PicoPlus AFM instrument (Molecular Imaging, Inc.) operating in non-contact mode. An aliquot of the sample, after a 25-fold dilution into the pH 2.7 buffer, was applied onto a freshly cleaved mica plate and incubated for 1 min. Then the mica surface was rinsed with water filtered with a 0.22- μ m filter (pH 2.7) and dried under vacuum for 45 min before scanning. The diameters of aggregates were determined from the Z-heights in AFM images, using the profile option of the program WSXM.⁵¹ For each mutant protein, 90–120 individual protofibrils were monitored. The height of each individual protofibril was determined as the mean of the heights determined along its length.

5,5'-Dithiobis (2-nitrobenzoic acid) assay

It was important to confirm that no disulphide bond formed during the protofibril formation process, even though DTT was always present. Cys3 (pH 2.7) was heated at 60 °C for 4 h, in the presence of 1 mM DTT, as it was heated during the measurement of the kinetics of protofibril formation. The protein was then passed through a HiTrap G-25 desalting column (GE) and equilibrated with buffer not containing DTT. The 5,5'-dithiobis (2-nitrobenzoic acid) assay, as described previously,⁵² was then carried out to confirm that there remained the expected one thiol group per protein molecule, as there was in the protein before conversion to protofibrils (data not shown). Clearly, no disulphide bond forms during the process of protofibril formation.

Analysis of kinetic data

The kinetic curves measured by any of the four probes were fitted to a single exponential equation to obtain the apparent rate constants. For each protein, the time constant measured from the kinetics of change in ThT fluorescence was defined as τ_{cc} , the time constant for conformational change (conversion).

Acknowledgements

We thank the members of our laboratory for discussion and for their comments on the manuscript. We thank K. C. Vishwanatha for assistance with the purification of the mutant proteins. This work was funded by the Tata Institute of Fundamental Research. The AFM images were collected at the Central Imaging Facility of the National Centre for Biological Sciences. S.K. was the recipient of a Senior Research Fellowship from the Council of Scientific and Industrial Research, Government of India. J.B.U. was the recipient of a J. C. Bose National Research Fellowship from the Government of India.

Supplementary Data

Supplementary data associated with this article can be found, in the online version, at [doi:10.1016/j.jmb.2008.11.033](https://doi.org/10.1016/j.jmb.2008.11.033)

References

- Chiti, F. & Dobson, C. M. (2006). Protein misfolding, functional amyloid, and human disease. *Annu. Rev. Biochem.* **75**, 333–366.
- Goldsbury, C., Frey, P., Olivieri, V., Aebi, U. & Müller, S. A. (2005). Multiple assembly pathways underlie amyloid- β fibril polymorphisms. *J. Mol. Biol.* **352**, 282–298.
- Smith, A. M., Jahn, T. R., Ashcroft, A. E. & Radford, S. E. (2006). Direct observation of oligomeric species formed in the early stages of amyloid fibril formation using electrospray ionisation mass spectrometry. *J. Mol. Biol.* **364**, 9–19.
- Lomakin, A., Chung, D. S., Benedek, G. B., Kirschner, D. A. & Teplow, D. B. (1996). On the nucleation and growth of amyloid β -protein fibrils: detection of nuclei and quantitation of rate constants. *Proc. Natl Acad. Sci. USA*, **93**, 1125–1129.
- Serio, T. R., Cashikar, A. G., Kowal, A. S., Sawicki, G. J., Moslehi, J. J., Serpell, L. *et al.* (2000). Nucleated conformational conversion and the replication of conformational information by a prion determinant. *Science*, **289**, 1317–1321.
- Xu, S., Bevis, B. & Arnsdorf, M. F. (2001). The assembly of amyloidogenic yeast Sup35 as assessed by scanning (atomic) force microscopy: an analogy to linear colloidal aggregation? *Biophys. J.* **81**, 446–454.
- Bitan, G., Kirkitadze, M. D., Lomakin, A., Vollers, S. S., Benedek, G. B. & Teplow, D. B. (2003). Amyloid β -protein (A β) assembly: A β 40 and A β 42 oligomerize through distinct pathways. *Proc. Natl Acad. Sci. USA*, **100**, 330–335.
- Modler, A. J., Gast, K., Lutsch, G. & Damaschun, G. (2003). Assembly of amyloid protofibrils *via* critical oligomers—a novel pathway of amyloid formation. *J. Mol. Biol.* **325**, 135–148.
- Hurshman, A. R., White, J. T., Powers, E. T. & Kelly, J. W. (2004). Transthyretin aggregation under partially denaturing conditions is a downhill polymerization. *Biochemistry*, **43**, 7365–7381.
- Carrotta, R., Manno, M., Bulone, D., Martorana, V. & Biagio, P. L. S. (2005). Protofibril formation of amyloid β -protein at low pH *via* a non-cooperative elongation mechanism. *J. Biol. Chem.* **280**, 30001–30008.
- Mukhopadhyay, S., Nayak, P. K., Udgaonkar, J. B. & Krishnamoorthy, G. (2006). Characterization of the formation of amyloid protofibrils from barstar by mapping residue-specific fluorescence dynamics. *J. Mol. Biol.* **358**, 935–942.
- Kumar, S., Mohanty, S. K. & Udgaonkar, J. B. (2007). Mechanism of formation of amyloid protofibrils of barstar from soluble oligomers: evidence for multiple steps and lateral association coupled to conformational conversion. *J. Mol. Biol.* **367**, 1186–1204.
- Petkova, A. T., Leapman, R. D., Guo, Z., Yau, W., Mattson, M. P. & Tycko, R. (2005). Self-propagating, molecular-level polymorphism in Alzheimer's β -amyloid fibrils. *Science*, **307**, 262–265.
- Hess, S., Lindquist, S. L. & Scheibel, T. (2007). Alternative assembly pathways of the amyloidogenic yeast prion determinant Sup35-NM. *EMBO Rep.* **8**, 1196–1201.
- Kad, N. M., Myers, S. L., Smith, D. P., Smith, D. A., Radford, S. E. & Thomson, N. H. (2003). Hierarchical assembly of β_2 -microglobulin amyloid *in vitro* revealed by atomic force microscopy. *J. Mol. Biol.* **330**, 785–797.
- Serpell, L. C., Blake, C. C. F. & Fraser, P. E. (2000). Molecular structure of a fibrillar Alzheimer's A β fragment. *Biochemistry*, **39**, 13269–13275.
- Heise, H., Hoyer, W., Becker, S., Andronesi, O. C., Riedel, D. & Baldus, M. (2005). Molecular-level secondary structure, polymorphism, and dynamics of full-length α -synuclein fibrils studied by solid-state NMR. *Proc. Natl Acad. Sci. USA*, **102**, 15871–15876.
- Sunde, M., Serpell, L. C., Bartlam, M., Fraser, P. E., Pepys, M. B. & Blake, C. C. F. (1997). Common core structure of amyloid fibrils by synchrotron X-ray diffraction. *J. Mol. Biol.* **273**, 729–739.
- Nelson, R., Sawaya, M. R., Balbirnie, M., Madsen, A. Ø., Riek, C., Grothe, R. & Eisenberg, D. (2005). Structure of the cross- β spine of amyloid-like fibrils. *Nature*, **435**, 773–778.
- Kad, N. M., Thomson, N. H., Smith, D. P., Smith, D. A. & Radford, S. E. (2001). β_2 -Microglobulin and its deamidated variant, N17D form amyloid fibrils with a range of morphologies *in vitro*. *J. Mol. Biol.* **313**, 559–571.
- Gosal, W. S., Morten, I. J., Hewitt, E. W., Smith, D. A., Thomson, N. H. & Radford, S. E. (2005). Competing pathways determine fibril morphology in the self-assembly of β_2 -microglobulin into amyloid. *J. Mol. Biol.* **351**, 850–864.
- Mališauskas, M., Zamotin, V., Jass, J., Noppe, W., Dobson, C. M. & Morozova-Roche, L. A. (2003). Amyloid protofilaments from the calcium-binding protein equine lysozyme: formation of ring and linear structures depends on pH and metal ion concentration. *J. Mol. Biol.* **330**, 879–890.

23. Caughey, B. & Lansbury, P. T. (2003). Protofibrils, pores, fibrils, and neurodegeneration: separating the responsible protein aggregates from the innocent bystanders. *Annu. Rev. Neurosci.* **26**, 267–298.
24. Kaye, R., Sokolov, Y., Edmonds, B., McIntire, T. M., Milton, S. C., Hall, J. E. & Glabe, C. G. (2004). Permeabilization of lipid bilayers is a common conformation-dependent activity of soluble amyloid oligomers in protein misfolding disease. *J. Biol. Chem.* **279**, 46363–46366.
25. Quist, A., Doudevski, I., Lin, H., Azimova, R., Ng, D., Frangione, B. *et al.* (2005). Amyloid ion channels: a common structural link for protein-misfolding disease. *Proc. Natl Acad. Sci. USA*, **102**, 10427–10432.
26. Collins, S. R., Dougllass, A., Vale, R. D. & Weissman, J. S. (2004). Mechanism of prion propagation: amyloid growth occurs by monomer addition. *PLoS Biol.* **2**(e321), 1582–1590.
27. Lomakin, A., Teplow, D. B., Kirschner, D. A. & Benedek, G. B. (1997). Kinetic theory of fibrillogenesis of amyloid β -protein. *Proc. Natl Acad. Sci. USA*, **94**, 7942–7947.
28. Baskakov, I. V., Legname, G., Baldwin, M. A., Prusiner, S. B. & Cohen, F. E. (2002). Pathway complexity of prion protein assembly into amyloid. *J. Biol. Chem.* **277**, 21140–21148.
29. Kodali, R. & Wetzel, R. (2007). Polymorphism in the intermediates and products of amyloid assembly. *Curr. Opin. Struct. Biol.* **17**, 48–57.
30. Surewicz, W. K., Jones, E. M. & Apetri, A. C. (2006). The emerging principles of mammalian prion propagation and transmissibility barriers: insight from studies *in vitro*. *Acc. Chem. Res.* **39**, 654–662.
31. DePace, A. H. & Weissman, J. S. (2002). Origins and kinetic consequences of diversity in Sup35 yeast prion fibers. *Nat. Struct. Mol. Biol.* **9**, 389–396.
32. Chien, P., DePace, A. H., Collins, S. R. & Weissman, J. S. (2003). Generation of prion transmission barriers by mutational control of amyloid conformations. *Nature*, **424**, 948–951.
33. Khurana, R. & Udgaonkar, J. B. (1994). Equilibrium unfolding studies of barstar: evidence for an alternative conformation which resembles a molten globule. *Biochemistry*, **33**, 106–115.
34. Swaminathan, R., Periasamy, N., Udgaonkar, J. B. & Krishnamoorthy, G. (1994). Molten globule-like conformation of barstar: a study by fluorescence dynamics. *J. Phys. Chem.* **98**, 9270–9278.
35. Juneja, J., Bhavesh, N. S., Udgaonkar, J. B. & Hosur, R. V. (2002). NMR identification and characterization of the flexible regions in the 160 kD molten globule-like aggregate of barstar at low pH. *Biochemistry*, **41**, 9885–9899.
36. Gast, K., Modler, A. J., Damaschun, H., Kröber, R., Lutsch, G., Zirwer, D. *et al.* (2003). Effect of environmental conditions on aggregation and fibril formation of barstar. *Eur. Biophys. J.* **32**, 710–723.
37. Naiki, H. & Gejyo, F. (1999). Kinetic analysis of amyloid fibril formation. *Methods Enzymol.* **309**, 305–318.
38. Chiti, F., Stefani, M., Taddei, N., Ramponi, G. & Dobson, C. M. (2003). Rationalization of the effects of mutations on peptide and protein aggregation rates. *Nature*, **424**, 805–808.
39. Hurler, M. R., Helms, L. R., Li, L., Chan, W. & Wetzel, R. (1994). A role for destabilizing amino acid replacements in light-chain amyloidosis. *Proc. Natl Acad. Sci. USA*, **91**, 5446–5450.
40. Chiti, F., Taddei, N., Bucciantini, M., White, P., Ramponi, G. & Dobson, C. M. (2000). Mutational analysis of the propensity for amyloid formation by a globular protein. *EMBO J.* **19**, 1441–1449.
41. Esler, W. P., Stimson, E. R., Jennings, J. M., Vinters, H. V., Ghilardi, J. R., Lee, J. P. *et al.* (2000). Alzheimer's disease amyloid propagation by a template-dependent dock-lock mechanism. *Biochemistry*, **39**, 6288–6295.
42. Lomakin, A., Benedek, G. B. & Teplow, D. B. (1999). Monitoring protein assembly using quasielastic light scattering microscopy. *Methods Enzymol.* **309**, 429–459.
43. Scheibel, T., Bloom, J. & Lindquist, S. L. (2004). The elongation of yeast prion fibers involves separable steps of association and conversion. *Proc. Natl Acad. Sci. USA*, **101**, 2287–2292.
44. Chimom, S., Shaibat, M. A., Jones, C. R., Calero, D. C., Aizezi, B. & Ishii, Y. (2007). Evidence of fibril-like β -sheet structures in a neurotoxic amyloid intermediate of Alzheimer's β -amyloid. *Nat. Struct. Mol. Biol.* **14**, 1157–1164.
45. Eghiaian, F., Daubenfeld, T., Quenet, Y., Audenhaege, M. V., Bouin, A., Rest, G. V. D. *et al.* (2007). Diversity in prion protein oligomerization pathways results from domain expansion as revealed by hydrogen/deuterium exchange and disulfide linkage. *Proc. Natl Acad. Sci. USA*, **104**, 7414–7419.
46. Pastor, M. T., Esteras-Chopo, A. & Paz, M. L. (2005). Design of model systems for amyloid formation: lessons for prediction and inhibition. *Curr. Opin. Struct. Biol.* **15**, 57–63.
47. Scheibel, T., Parthasarathy, R., Sawicki, G., Lin, X., Jaeger, H. & Lindquist, S. L. (2003). Conducting nanowires built by controlled self-assembly of amyloid fibers and selective metal deposition. *Proc. Natl Acad. Sci. USA*, **100**, 4527–4532.
48. White, S. H. & Wimley, W. C. (1999). Membrane protein folding and stability: physical principles. *Annu. Rev. Biophys. Biomol. Struct.* **28**, 319–365.
49. Street, A. G. & Mayo, S. L. (1999). Intrinsic β -sheet propensities result from van der Waals interactions between side chains and the local backbone. *Proc. Natl Acad. Sci. USA*, **96**, 9074–9076.
50. Jha, S. K. & Udgaonkar, J. B. (2007). Exploring the cooperativity of the fast folding reaction of a small protein using pulsed thiol labeling and mass spectrometry. *J. Biol. Chem.* **282**, 37479–37491.
51. Horcas, I., Fernández, R., Gómez-Rodríguez, J. M., Colchero, J., Gómez-Herrero, J. & Baro, A. M. (2007). WSXM: a software for scanning probe microscopy and a tool for nanotechnology. *Rev. Sci. Instrum.* **78**, 013705.
52. Ramachandran, S. & Udgaonkar, J. B. (1996). Stabilization of barstar by chemical modification of the buried cysteines. *Biochemistry*, **35**, 8776–8785.